行政院國家科學委員會專題研究計畫 成果報告

高溫氣冷式核子反應器與產氫系統先期研究--子計畫二：建立及應用數值方法於氦冷式核子反應器之爐心熱流分析

研究成果報告(精簡版)

計 畫 類 別 ： 整合型
計 畫 編 號 ： NSC 96-2221-E-216-023-
執 行 期 間 ： 96 年 08 月 01 日至 97 年 09 月 30 日
執 行 單 位 ： 中華大學機械工程學系

計 畫 主 持 人 ： 牛仰堯

報 告 附 件 ： 出席國際會議研究心得報告及發表論文

處 理 方 式 ： 本計畫涉及專利或其他智慧財產權，2 年後可公開查詢

中 華 民 國 97 年 09 月 24 日

行政院國家科學委員會專題研究計劃成果報告

建立及應用數值方法於氦冷式核子反應器之爐心熱流分析(Ⅰ)

計畫編號：NSC96－2323－E－216－023

執行期間：九十六年八月一日至九十七年七月三十一日

主持人: 牛仰堯 中華大學機械系

共同主持人：錢景常 馮玉明　清華大學工程與系統科學系

關鍵字: 高溫核子反應器、氦氣冷卻、可壓縮熱流模擬

Key words: High-Temperature Reactor, helium cooling, compressible flow, numerical heat transfer simulation

一.中文摘要

高溫核子反應器的概念於1980 年代首先在德國被提出。然後許多國家展開相關設計與發展。現行發展高溫核子反應器是一模組化的球體床核子反應裝置，並藉由氦氣冷卻將高熱量從反應器核心帶到蒸汽產生器，並維持反應器正常的運轉。因此反應器爐心熱流場模擬，將有助於高溫核子反應器冷卻系統的設計，以確保其正常工作及安全。

第一年我們使用多孔性模式及半經驗公式作熱流模擬；以中國高溫核子反應器為本之各項設計參數，包括固體性質、流體性質，以計算流場、密度分佈及溫度場。

二.英文摘要.

The concept of modular High-Temperature Reactors (HTR) was proposed firstly in Germany in the 1980th. Then, many countries started the design and development on modular HTR The current ongoing generation of HTR is a pebble bed, graphite moderated modular reactor which is cooled by helium gas and the spherical fuel elements are piled into a pebble bed. Helium coolant is a key component of the high temperature gas-cooled reactor which assures the thermal energy transfer from the reactor core to the steam generator. The thermal hydraulic calculations of the high temperature gas-cooled-test module are among the most important indications to judge the reactor performance under design conditions. To simulate the flow and heat transport within the core, the study will be focused on the development of a numerical tool for the safety analysis of high-power HTRs. Present study adopts the porous medium model and semi-empirical formula to perform the thermohydraulic analysis. The design parameters including physical properties are referenced to HTR-10 to compute the flowfield, density distribution, and temperature field.

三.計畫緣由與目的

三離島以及車諾比事件發生後，長久以來國人籠罩在一片反核聲浪中，但又不得不仰仗它對人們帶來的生活便利以及經濟效益。在化石燃料宣告將用盡之時，且未有新的能源替補之際。相信核能發電還是國人最需要的能源之一。在此為了重拾人們對核能發電的信心，一些開發中國家或已開發國

家，尤以歐美、中、俄、印、日、韓、南非等新興國家已積極地向核能工業頻頻招手，研發一些高安全且高效率的新型反應器。

我們針對中國北京清華大學所建設的高溫氣冷式反應器[1](HTR-10) 如圖 1，此反應器以氦氣作為冷卻劑石墨為緩和劑，且它是一座可以不停更換燃料的反應器，可以省去不少更換燃料時所造成的經濟損耗與安全疑慮。一座高溫氣冷式反應器裡面包含了 27000 顆球體，球體分為有燃料和無燃料部份，裝填進入爐心比例分別為 57%和 43%。如圖 2 每顆燃料球直徑為 6cm外層是以 0.5cm的石墨包覆內部含有近千顆的燃料粒子，而無燃料也就是石墨球即內部沒有燃料粒子。

整座反應器球床直徑為180cm，平均高度為197cm，燃料設計的平均燃耗為80000MW$_d$ t^{-1}，選用石墨作為主要的反應器爐心結構材料。位於外層反射體上有兩個獨立的反應器停機系統，控制棒系統和吸收中子系統，此兩系統有能力控制反應器至完全停機之條件。反應器有著極大的負溫度系數使得衰變熱移除不需要任何的氦氣冷卻劑流過，即使關閉氦氣循環系統也能在功率運轉條件下使反應器安全停機。

我們將此次研究用多孔性模式及半經驗公式作流模擬；以中國HTR-10設計為本，確定各項參數以計算流場、密度分佈及溫度場。模擬選用的固體性質如表2，而流體性質如表3第二部份利用多孔性半經驗公式模擬高溫氣冷式反應器球床部份。

四. 四.結果與討論

在此我們使用fluent做為分析軟體。模擬所有的流動，都是解連續和動量守恆方程式。對於包括熱傳導或可壓縮性的流動，需要解能量守恆的附加方程式。若為物種混合以及反應的流動，則需要解物種方程式。當流動是紊流時，還要再解附加的紊流方程式。

多孔介質模型所具有的阻力經由半經驗公式定義。事實上多孔性介質不過是在動量方程中添加了動量損失而已。在此選用的多孔性之阻力半經驗公式為Ergun方程式[5]。Ergun方程式由兩部分組成，前項是黏滯阻力，後項為形狀阻力。

最簡單且完整的紊流模型是兩個方程式的模型，要求解兩個變數，速度和長度尺度。在標準 k- ε 模型自從被 Launder and Spalding[6]提出之後，就變成工程流場計算中主要的工具了。它是個半經驗的公式，是從實驗現象中所總結出來的。適用範圍廣且有合理的精度，這就是為什麼它在工業流場和熱交換模擬中有如此廣泛的應用了。

連續方程式：

$$\frac{\partial(\gamma\rho)}{\partial t}+\nabla\cdot(\gamma\rho\vec{v})=0 \qquad (1)$$

其中：

ρ = density

$\vec{v}$ = velocity

γ = porosity

動量方程式：

$$\frac{\partial(\gamma\rho\vec{v})}{\partial t}+\nabla\cdot(\gamma\rho\vec{v}\vec{v})=-\gamma\nabla p+\nabla\cdot(\gamma\vec{\tau})+\gamma\rho\vec{g}-\left(\frac{\mu}{\alpha}+\frac{C_2\rho}{2}|\vec{v}|\right)\vec{v} \qquad (2)$$

Ergun方程式：

$$\frac{|\Delta p|}{L}=\frac{150\mu}{D_p^2}\frac{(1-\gamma)^2}{\gamma^3}v_\infty+\frac{1.75\rho}{D_p}\frac{(1-\gamma)}{\gamma^3}v_\infty^2 \qquad (3)$$

$$\alpha=\frac{D_p^2}{150}\frac{\gamma^3}{(1-\gamma)^2} \qquad (4)$$

$$C_2=\frac{3.5}{D_p}\frac{(1-\gamma)}{\gamma^3} \qquad (5)$$

其中：

$\vec{\tau}$ = stress tensor

p = static pressure

$\rho\vec{g}$ = gravitational body force

μ = viscosity

D_p = mean particle diameter
L = bed depth
α = permeability
C_2 = inertial loss coefficient

能量方程式：

$$\frac{\partial}{\partial t}(\rho E) + \nabla \cdot (\vec{v}(\rho E + p)) = \nabla \cdot \left(k_{\text{eff}} \nabla T - \sum_j h_j \vec{J}_j + (\bar{\bar{\tau}}_{\text{eff}} \cdot \vec{v}) \right) + S \quad (6)$$

$$\frac{\partial}{\partial t}(\gamma \rho_f E_f + (1-\gamma)\rho_s E_s) + \nabla \cdot (\vec{v}(\rho_f E_f + p)) = \nabla \cdot \left[k_{\text{eff}} \nabla T - \left(\sum_i h_i J_i \right) + (\bar{\bar{\tau}} \cdot \vec{v}) \right] + S \quad (7)$$

其中：

$$E = h - \frac{p}{\rho} + \frac{v^2}{2}$$

$$\nabla \cdot \left[\sum_{i=1}^{n} h_i \vec{J}_i \right] = \text{Species Transport}$$

E_f = total fluid energy
E_s = total solid medium energy

k_{eff} = effective thermal conductivity of the medium
S = fluid enthalpy source term

紊流中的質量擴散：

$$\vec{J}_i = -\left(\rho D_{i,m} + \frac{\mu_t}{\text{Sc}_t} \right) \nabla Y_i \quad (8)$$

其中：

Sc_t = turbulent Schmidt number = 0.7

μ_t = turbulent viscosity

層流有限速率模型：

$$R_i = M_{w,i} \sum_{r=1}^{N_R} \hat{R}_{i,r} \quad (9)$$

其中：

$$\sum_{i=1}^{N} \nu'_{i,r} \mathcal{M}_i \underset{k_{b,r}}{\overset{k_{f,r}}{\rightleftharpoons}} \sum_{i=1}^{N} \nu''_{i,r} \mathcal{M}_i$$

$$\hat{R}_{i,r} = \Gamma \left(\nu''_{i,r} - \nu'_{i,r} \right) \left(k_{f,r} \prod_{j=1}^{N_r} [C_{j,r}]^{\eta'_{j,r}} - k_{b,r} \prod_{j=1}^{N_r} [C_{j,r}]^{\eta''_{j,r}} \right)$$

$$\Gamma = \sum_{j}^{N_r} \gamma_{j,r} C_j$$

$$k_{f,r} = A_r T^{\beta_r} e^{-E_r/RT}$$

$$K_r = \exp\left(\frac{\Delta S_r^0}{R} - \frac{\Delta H_r^0}{RT} \right) \left(\frac{p_{\text{atm}}}{RT} \right)^{\sum_{r=1}^{N_R} (\nu''_{j,r} - \nu'_{j,r})}$$

$$k_{b,r} = \frac{k_{f,r}}{K_r}$$

$$\frac{\Delta S_r^0}{R} = \sum_{i=1}^{N} \left(\nu''_{i,r} - \nu'_{i,r} \right) \frac{S_i^0}{R}$$

$$\frac{\Delta H_r^0}{RT} = \sum_{i=1}^{N} \left(\nu''_{i,r} - \nu'_{i,r} \right) \frac{h_i^0}{RT}$$

N_r = number of chemical species in reaction r
$C_{j,r}$ = molar concentration of each reactant and product species j in reaction r (kgmol/m^3)
$\eta'_{j,r}$ = forward rate exponent for each reactant and product species j in reaction r
$\eta''_{i,r}$ = backward rate exponent for each reactant and product species j in reaction r

A_r = pre-exponential factor (consistent units)
β_r = temperature exponent (dimensionless)
E_r = activation energy for the reaction (J/kgmol)
R = universal gas constant (J/kgmol-K)

標準k-ε 紊流方程式：

$$\frac{\partial}{\partial t}(\rho k) + \frac{\partial}{\partial x_i}(\rho k u_i) = \frac{\partial}{\partial x_j} \left[\left(\mu + \frac{\mu_t}{\sigma_k} \right) \frac{\partial k}{\partial x_j} \right] + G_k + G_b - \rho\epsilon - Y_M \quad (10)$$

$$\frac{\partial}{\partial t}(\rho \epsilon) + \frac{\partial}{\partial x_i}(\rho \epsilon u_i) = \frac{\partial}{\partial x_j} \left[\left(\mu + \frac{\mu_t}{\sigma_\epsilon} \right) \frac{\partial \epsilon}{\partial x_j} \right] + C_{1\epsilon} \frac{\epsilon}{k} (G_k + C_{3\epsilon} G_b) - C_{2\epsilon} \rho \frac{\epsilon^2}{k} \quad (11)$$

其中：

$C_{1\epsilon} = 1.44, \quad C_{2\epsilon} = 1.92, \quad C_\mu = 0.09, \quad \sigma_k = 1.0, \quad \sigma_\epsilon = 1.3$

k = kinetic energy
ϵ = rate of dissipation
G_k = generation of turbulence kinetic energy due to the mean velocity gradients
G_b = generation of turbulence kinetic energy due to buoyancy
Y_M = contribution of the fluctuating dilatation in compressible turbulence to the overall dissipation rate
$C_{1\epsilon}, C_{2\epsilon}, C_{3\epsilon}$ = constants.
$\sigma_k, \sigma_\epsilon$ = turbulent Prandtl numbers for k and ε

根據以上之多孔性的模式，模擬之孔隙度為0.59，產生 2231747 w/m^{3}之功率。以計算流場及溫度場。

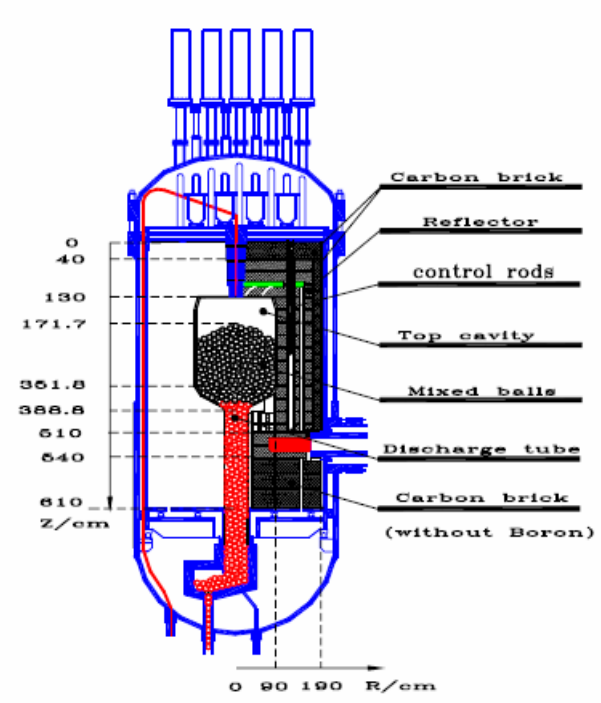

圖1：高溫氣冷式反應器垂直斷面圖

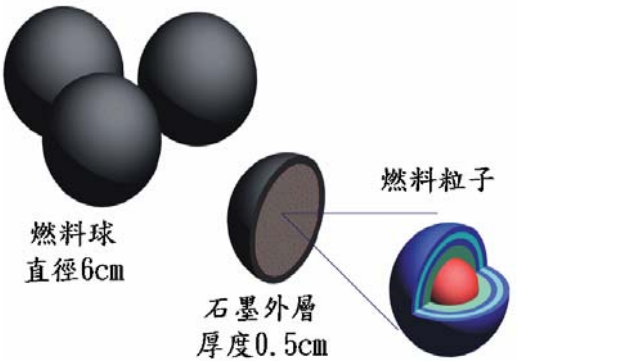

圖 2：燃料球示圖 2：燃料球示意圖

模擬HTR-10 在全功率運轉下的流場

HTR-10 之設計參數如表 1，在此我們模擬HTR-10 爐心之建模如圖 3。在圖 4 中core-top為氦氣最先流入的地方溫度最低處，內部沒有燃料球；core-fuel為氦氣加熱的區域內部包含了燃料球與石墨球，流體經過此區域時會產生流阻；discharge-tube是把用過燃料排出的區域，在此區域內僅剩下燃料用盡的石墨球故不會使氦氣溫度再提高，但由於含有石墨球的關係所以會產生與core-fuel相同之流阻； core-exit 此區域為收集core-fuel加熱後的氦氣； SG-pipe它是一段連接爐心與蒸汽產生器的一段管路。

在此用固定功率以輸出功率為 2231747 w/m^3 之狀況。(圖 5 為 HTR-10 全功率運轉下之功率密度分佈)以計算流場及溫度場。模擬選用的固體性質如表 2，而流體性質如表 3

表 1：HTR-10 設計參數[1]

Physical parameter	unit	Value
Reactor core		
Core equivalent diameter	cm	180
Core equivalent height	cm	196.5
Height of the top cavity in the core	cm	42
Thickness of the top reflector	cm	90
Height of the bottom cone reflector	cm	38
Thickness of the bottom reflector	cm	121
Equivalent thickness of the side reflector	cm	78
Density of the reflector graphite	g•cm^{-3}	1.76
Impurity content of equivalent to natural boron in the graphite	ppm	4.8
Thickness of the top carbon brick with natural boron	cm	40
Thickness of the bottom carbon brick with natural boron	cm	30
Thickness of the bottom carbon brick without natural boron	cm	70
Equivalent thickness of the side carbon brick with natural boron	cm	22
Density of the carbon brick	g•cm^{-3}	1.59
Mass content of B_4C in carbon brick with natural Boron	%	5
Number of control rods in side reflector		10
Number of absorber ball units in side reflector		7
Fuel element		
Volumetric filling factor of the fuel element		0.61
Nuclear fuel		UO_2
Heavy metal loading per fuel element	g	5
Enrichment of fresh fuel element	%	17
Diameter of the fuel element	cm	6
Diameter of fuel zone in the fuel element	cm	5

表 2：固體性質

	石墨(C)	鈾(U)
密度 (kg/m^3)	2267	19050
比熱 C_p(J/kg-k)	Piecewise-linear	120
熱傳導度 (w/m-k)	Piecewise-linear	27.6

表 3：流體性質

	氦氣(H_e)
比熱C_p(J/kg-k)	5193.087
熱傳導度(w/m-k)	Piecewise-linear
黏滯係數 (kg/m-s)	Piecewise-linear
分子量 (kg/kgmol)	4

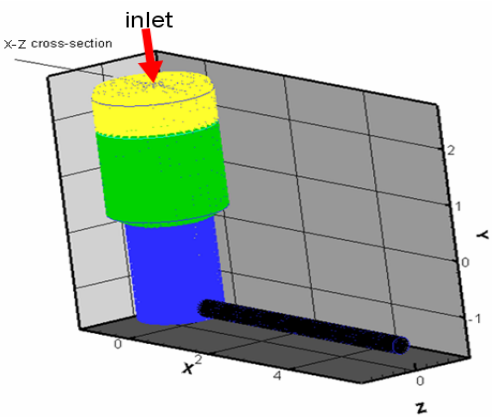

圖 3：HTR-10 爐心部分模擬圖

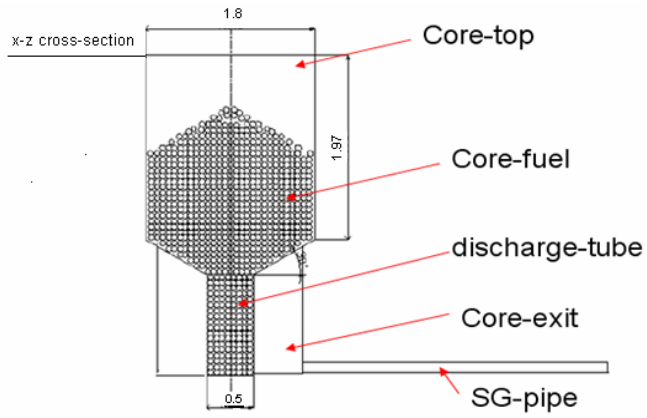

圖 4：HTR-10 爐心內部構造與命名

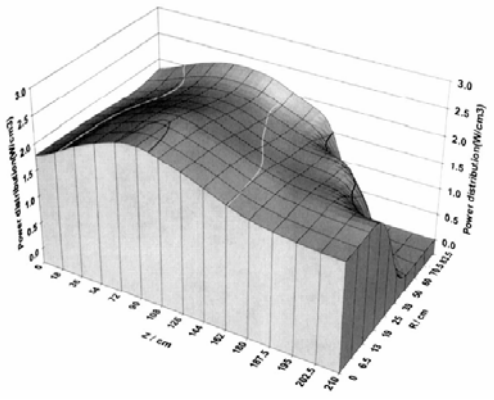

圖 5：HTR-10 全功率運轉下之功率密度分佈[3]

流體通過多孔性區域速度上升，離開時速度下降看不出球體周圍之變化。圖 6 是流體通過多孔性區域時速度上升，離開多孔性區域時速度下降，看不出個別燃料球體周圍之變化。可以清楚看出利用多孔性近似速度無太大差異性，速度介於 1.2m/s~0.6m/s 之間。

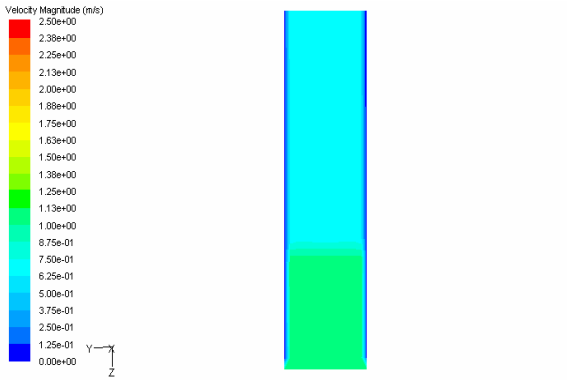

(a)

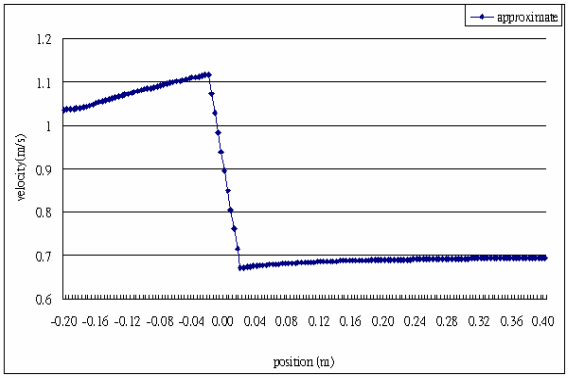

(b)

圖 6：多孔性模擬之(a)速度等值圖 (b) 速度數值圖

圖 7 觀察到由於氦氣逐漸加熱的關係，使得溫度逐漸上升之趨勢。圖 8 呈現出密度之等值圖，計算方式是根據 ideal-gas。由於模型之操作壓力為 3Mpa 所以計算的壓差影響不大，整體趨勢是與溫度成反比來表示，溫度愈高則密度愈小。

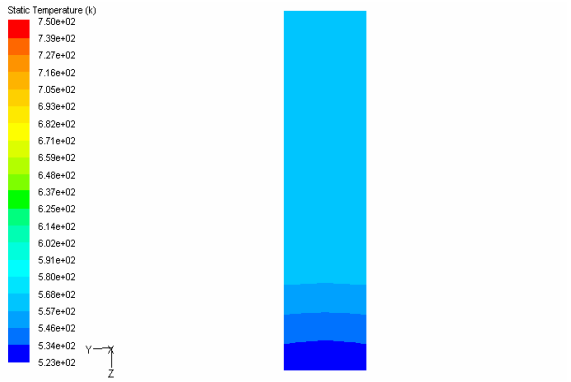

(a)

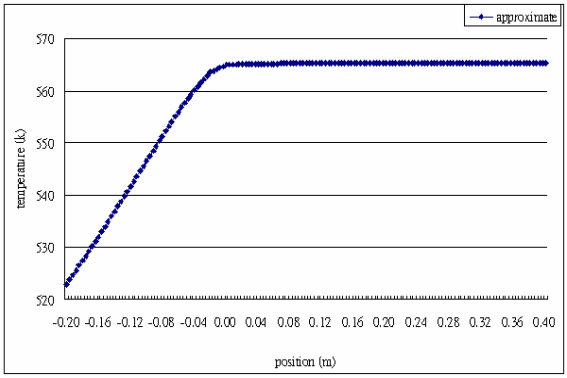

(b)

圖 7：多孔性模擬之（a)溫度等值圖（b）溫度數值圖

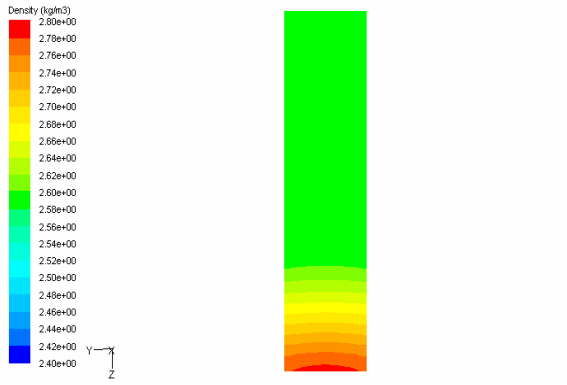

(a)

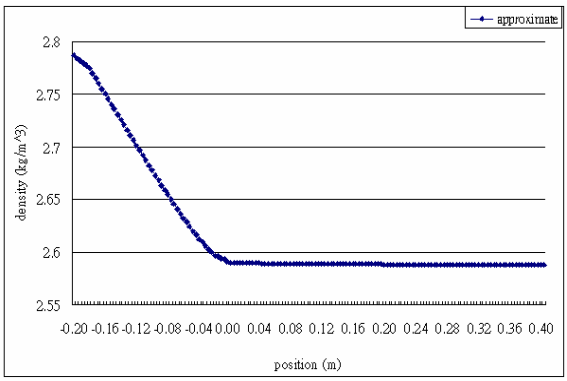

(b)

圖 8： 多孔性模擬之(a) 密度等值圖(b)密度數值圖

參考文獻：

1. Jing Xingqing, Yang Yongwei ,PHYSICAL DESIGNS AND CALCULATIONS FOR THE FIRST FULL POWER OPERATION OF THE 10MW HIGH TEMPERATURE GASCOOLED REACTOR—TEST MODULE (HTR-10) ,2004
2. Margaret and Richard, FLUID FLOW ANALYSIS IN A PEBBLE BED MODULAR REACTOR USING RANS TURBULENCE MODELS, Proceedings of the 16th International Conference on Nuclear Engineering, 2008
3. Zuying Gao , Lei Shi Thermal hydraulic calculation of the HTR-10 for the initial and equilibrium core,2002
4. Zuying GAO, Chunyun WANG,Baoyan LI, TRANSIENT ANALYSIS OF WATER INGRESS INTO THE HTR-1O HIGH TEMPERATURE GAS COOLED TEST REACTOR
5. S. Ergun. Fluid Flow through Packed Columns. Chem. Eng., 1952
6. B. E. Launder and D. B. Spalding. Lectures in Mathematical Models of Turbulence. Academic Press, London, England, 1972.

The 6th IASME/WSEAS International Conference on FLUID MECHANICS and AERODYNAMICS 心得報告

中華大學機械系
報告人：牛仰堯

參加國際性會議不僅可以了解國外在相關領域的最新研究發展狀況， 同時也是與國外學者專家技術交流最直接最具經濟效益的方法之一。因為一個成功的研討會，可以在短短的幾天中，聚集了來自各地達數百，甚至數千位學者專家於同一地點，做面對面直接的討論與溝通。 因此為求得在最短時間內獲取最新的資訊，參加謹慎選擇的國際性研討會，是最值得的。 本次 IASME/WSEAS 國際流體力學與氣體動力學研討會於希臘羅德島舉行，有來自各地的相關專家與學者，包括大學教授、研究人員、各國家實驗室的專職人員、工業界相關研究人員出席或發表論文。在會場上並有出版商提供各種流體力學平行計算相關專業書刊與資料，以及最新 CFD 電腦模擬所需的軟體所需的各項器材之展覽。

本次會議於 8 月 19 日開始辦理報到註冊，主辦單位同時展示一些會議相關論文集及專業書刊，並有部份工作人員舉行會議前之準備集會。接下來的 3 天為正式的會議，包括專題演講 6 個邀請演講、專題討論及論文發表等議程。 由大會依專業細分為 8 大項，論文發表以 3 個場地同時進行，共計有 18 場，每場約有 5-6 篇論文，會場外的大廳有軟體廠商、出版商與實驗器材廠商的展示及研究生之論文成果展。大會的子題包括了：Mechanical and Aerospace Engineering, Industrial and Environmental Engineering, Medical and Biological Applications Atmospheric and Ocean Modeling, Combustion,Turbulence, Acoustics, Plasma Dynamics, Design Optimization. 由於場次眾多，個人僅能選擇性的參與 Two-phase flow 論文發表觀摩。大本次會議台灣除筆者外，另外有成功大學教授參與論文發表。. 由本次研討會所發表的 90 餘篇論文可以看出流體力學與氣體動力學領域發展之現況。此次亞洲學者參與的人數並不踴躍但由此研討會可看出歐洲在流體力學與氣體動力學之研究頗為深入，台灣應參與歐洲計算力學之研討會增進彼此了解，對於促進國內科技研究，提升學術水準有莫大的助益。本次大會共安排了 8 月 21 日的的晚宴世界各地的學者專家促進情感交流。

攜回資料名稱及內容

1. IASME/WSEAS 會議程手冊
2. IASME/WSEAS 研討會論文 CD 集

The 6th IASME/WSEAS International Conference on FLUID MECHANICS and AERODYNAMICS
Rhodes (Rodos) Island, Greece, August 20-22, 2008

Numerical Simulation Cavitated Flows Based on preconditioning Tecnique

Yang-Yao Niu[1], Yung Xsien-Chiu and Yong–Cheng Chuang
Institute of Mechanical Engineering Chung-Hua University, Hsin- Chu, Taiwan, ROC.
yniu@chu.edu.tw

Abstract: - This paper is to continue our previous work (Niu, 2006) on solving a locally homogeneous two-phase mixture for water-steam flows using a modified AUSMDV scheme. Here, a simple unified hybrid flux splitting algorithm for multi-phase flows with arbitrary equation of state based on the preconditioning derived from AUSMD scheme (Wada and Liou, 1997) and flux difference scheme (Weiss and Smith, 1995) is proposed presented. In the cavitated flow model, we consider a homogeneous two-phase mixture model with the assumption of kinematics and thermodynamics equilibriums. The thermodynamics behaviors of liquid phase, vapor phase and their phase transitional process are described by a temperature dependent hybrid equation of state which includes an empirical formula of water-vapor saturation process. The preconditioning strategy is utilized to reformulate the compressible mixture type Navier-Stokes equations coupling with a condensation-vaporization convective equation to be hyperbolic at all-speed. The proposed robust low diffusion upwind flux splitting is shown to be robust in the simulation of several general cases at steady and transient states which include two-phase nozzles, shock tubes and low-speed cavitating flows over a 3D blunt body.

Key-Words: Cavitation, Phase change, Multi-Phase Flow, Riemann solver

1 Introduction

The development of high-resolution algorithms to simulate perfect gas flow problems has achieved tremendous progress during the past 20 years. Based on successful resolutions of shock waves and discontinuities in single phase flows, these successful numerical techniques are currently applied on the simulation of the compressible hydrodynamics flow problems which contain the complicated phase interfaces, material discontinuities and phase transition behaviors. These multi-phase transitioning flow phoenomena, widely seen in the power cooling system, the fuel transport system, the underwater cavitation, recently attract many efforts in developing the related numerical models. As we know, the low Mach number hydrodynamics usually is considered as incompressible. The incompressible flow assumption always ignores the density variation and the thermodynamics property of pressure. In the formulation of incompressible flows, the hyperbolicity is no longer considered. Consequently, the related propagation of the acoustic waves and the compressibility are ignored in the simulation. As noted in [1, 2], cavitation is one of important phenomena in compressible hydrodynamics. Cavitation is well known to associate with three aspects: formation, growth and collapse of bubbles within the body of a liquid due to the process of nucleation in a liquid flow where the pressure falls below the vapor pressure. During the liquid-vapor phase transitions, vapor bubbles or cavities in a fluid usually collapse at a high frequency and generate high pressure gradients and acoustic waves to erode microscopic pieces of metal if they are close to the metallic wall. Therefore, the acoustic waves induced by abrupt density variation and the pressure drop during the phase change of cavitating flows would be beyond the scope of the incompressible flow assumption.

A primary issue in the simulation of compressible cavitated flow is how to accurately simulate multi-acoustic phenomena [3, 4]. The speed of sound in two-phase mixtures can be extremely low compared to the sound speeds in the individual component phases. Thus, multiphase flows are frequently characterized by local regions, wherein the flow may be transonic or even supersonic with the presence of shocks, although the bulk of the flow may remain essentially incompressible. This situation presents a big challenge, especially to the numerical stability of algorithms. Several numerical methods have been proposed in the past in order to

[1] professor

accurately capture the fluid interfaces for the two phase flows, such as the VOF method [5, 6], the level set method [7-10], the front tracking method [11] and the interface capturing method [12-16]. However, compressibility effects and phase transitions were not considered in most of the past numerical works. It is well known that the
coupling between the liquid pressure and density field is very weak in most of the current compressible liquid flow models, especially in the nearly incompressible regime. The variation in density is extremely insignificant even a very large pressure gradient is imposed on the flow. On the contrary, small numerical errors in density field may result in violent jumps in the prediction of pressure waves, the phase interfaces and discontinuities which are the prominent phenomena in cavitation. In addition, in high-speed cavitated flows, strong temperature dependence on variations of pressure and density induced by high kinetic energy transfer always produce complicated multi-acoustic phenomena which make the resolutions of interfaces inaccuracy. In the past works on compressible cavitated flow models, Saurel and Cocchi [13] adopted high-order central finite volume discretization with artificial dissipations terms to compute the high-speed underwater cavitated flow problems. They first proposed an effective temperature dependent liquid-vapor phase change model with a combined EOS to represent the thermodynamics properties of the water and vapor and the related phase transition. The hybrid equation of state proposed by Saurel and Cocchi is widely used and modified in the many other studies [15-17]. However, in order to remove the erroneous temperature rise appearing in the conservative formulation, Saurel and Cocchi used a non-conservative energy equation and a shock detector to revert scheme to be a conservative formulation near shocks. The solution technique employed is either unsusceptible to the erroneous rarefaction temperature or lose conservation property of energy in the subsonic flow regime. To overcome the deficiency in the works of Saurel and Cocchi, the conservative homogeneous equilibrium multi-fluid approaches solving by upwinding type low-diffusion flux splitting methods improve the simulation in the works [15-18]
In our previous work [17, 18] on resolution of air-water interface among two-phase non-cavitated flows under 1:1000 density ratio of air to water was performed. We suggested that the computation of the dynamics of multi-component flow is performed on the extended Euler equation with VOF model and using the interface capturing type AUSM or AUSMDV [19, 20] scheme. The conservation form is considered in the model equation. As we know, the AUSM or AUSMDV has been be as accurate as Roe's or Osher's approximate Riemann solvers without the cost of field-by-field wave decompositions. Of particular, the importance is the ability of the scheme to capture contact discontinuities exactly, thereby making the scheme very attractive for viscous flow computations. Extension of the AUSM scheme to multi-phase flow was first performed by Edwards et al [15], based on the homogeneous equilibrium mixture model which is formally identical to the Euler equations of gas dynamics, with arbitrary EOS. Also his work done by the LDFSS-2001 [16] has been extensively applied on more sophisticated high-speed underwater flow problems. Recently, Chang and Liou [21] proposed AUSM+up incorporating with stratified flow approach to solve a non-equilibrium two-phase model. Their proposed approaches demonstrated robustness and high-order accuracy in all benchmark cases, excepting the air-water shock tube problem with nearly pure air and water separated by a diaphragm. Their remedy is to remove unnecessary numerical oscillating errors was using exact Riemann solver instead of AUSM+up to simulate the liquid-gas interfaces between pure air and water. In our previous calculations [18], the AUSM and AUSM+up was shown to yield oscillatory solutions based on the liquid fluid is represented by the stiffened gas model (or Tammann's model). The stiffness of the EOS for the liquid makes the AUSM+ scheme unable to resolve the pressure waves well. However, the suggested AUSMDV demonstrated excellent accuracy compared with exact solutions and exhibits oscillation-free material interfaces in several one-dimensional two-phase test cases. Also, the pressure-velocity coupling dissipation term in AUSMDV is also suggested to modify AUSM+up for solving an unsteady mixture model with the phase transition model, The proposed modification of AUSM+ is shown to enhance accurate resolution of phase interfaces and liquid pressure waves in the unsteady cavitated shot tube problems and achieve robust calculations of unsteady external cavitated flows after comparing with validated data.

Here, we would like to extend our efforts on the extension of the liquid-gas mixture model with the VOF model similar as [16, 23-27]. In this work, a temperature dependent water-vapor phase change model based on a hybrid equation of state as [16] combined with a convection equation of the vaporization and condensation is utilized. The accuracy of the proposed AUSMDV, LDFSS-2001

and AUSM+up based on preconditioning strategy are performed for the comparison.

2 Problem Formulation

In this study, a two-dimensional two phase mixture model with a saturation model and a precondition matrix is proposed here. In the numerical strategy, a TVD type Runge-Kutta Time accurate scheme is used to solve the model equation to keep the numerical stability. In the spatial differencing, the interface conservative variables are determined through a third order accurate MUSCL interpolation [27] with the minmod limiter. Subsequently, the flux splitting based on an improved AUSMDV to discretize the convective fluxes of, gas mass, total mass, momentum, energy, respectively. In addition, to model the phase transitions among the steam-water mixture, three equations of state for water, vapor and saturation states modified from [18, 26] based on local phase equilibrium are selected together to yield a smooth link at the so-called spinodal points, the extreme points on the both sides of the saturation zone in the temperature-pressure diagram, also accurately cover the range ($27315K \le T \le 62315K$ & $ps(T) \le p \le 100MPa$). They are briefly described as the following sections:

2.1 Governing Equations

For all-speed flow regime, a preconditioning strategy is to extend the functionality of existing codes for fully compressible flows to almost incompressible flows. Applying the preconditioning method to Eq. (1), we obtain 2-D preconditioned governing equations with unknown variable vectors $\boldsymbol{W} = [p, u, v, w, T, Y]$ written in curvilinear coordinates as follows [13]: Here we used the preconditioning techniques of Weiss and Smith which introduced artificial time scale τ and a reconditioning matrix to rescale the original governing equations A mixture type two-phase compressible Navier-Stokes Equations conjunction with a mass-fraction (Y) type cavitation model and a water-vapor saturation model based on hybrid equations of state are chosen here. They are demonstrated as

$$\Gamma \frac{\partial}{\partial t}\iiint W dV + \oiint (F - F_v) dA = S \qquad (1)$$

where the primitive variable vector Q and the invisicid fluxes E and the viscous term E_v are

$$W=\begin{pmatrix} p \\ u \\ v \\ w \\ T \\ Y \end{pmatrix} \; ; \; E=\frac{1}{J}\begin{pmatrix} \rho U \\ \rho uU + n_x p \\ \rho vU + n_y p \\ \rho wU + n_z p \\ \rho HU \\ \rho YU \end{pmatrix} \; ; \; S=\begin{pmatrix} 0 \\ 0 \\ 0 \\ 0 \\ 0 \\ \dot{m}_- + \dot{m}_+ \end{pmatrix} \qquad (2)$$

where U are represented as

$$U = n_x u + n_y v + n_z w$$

and total energy and total enthalphy and enthalpy are expressed respectively as

$$E = H - p/\rho \; ; \; H = h + |U_i|^2/2 \; ; \; h = C_p T \qquad (i = 1,2,3)$$

In addition, S is a vector of finite-rate source terms used to specify rate of vapor production and destruction.
$\dot{m}^+ = C_{prod}\rho_v \alpha_l^2 (1-\alpha_l)/t_\infty$ and
$\dot{m}^- = C_{dest}\rho_l \alpha_v MIN(0, P - P_v)/t_\infty$; respectively.

$$\dot{m}_l = \left(\frac{c_{\text{evap}}}{t_\infty}\right)\alpha_l \text{Min}[0, p - p_v]$$
$$\dot{m}_g = \left(\frac{c_{\text{prod}}}{t_\infty}\right)\alpha_g \text{Max}[0, p - p_v] \qquad (3)$$

Here, t_∞ is the characteristic time and the saturation pressure p_v is defined as :
For the present work, $C_{prod} = 8\times10^1, C_{dest} = 1\times10^4$, $t_\infty = L/U_\infty$. The total energy can be expressed as

$$E = \sum_{i=1}^{m} \alpha_i \rho_i e_i + \frac{1}{2}\alpha_i \rho_i \left(u^2 + v^2\right) \qquad (4)$$

where u and v are the components of velocity on Cartesian coordinates respectively. The gas-phase density, ρ_g, is defined as the mass of the gaseous mixture divided by the volume occupied by the gaseous mixture and the mass fraction of the gaseous mixture is denoted as by Y. With

$$\rho Y_g = \rho_g \alpha_g \qquad (5)$$

Also the mixture density and internal energy are respectively denoted as

$$\rho=\alpha_g\rho_g+\alpha_l\rho_l \quad ; \quad e=\alpha_g e_g+\alpha_l e_l \qquad (6)$$

and the relationships of the mixture bulk density and enthalpy with mass fraction can be expressed by

$$\frac{1}{\rho}=\frac{Y_g}{\rho_g}+\frac{Y_l}{\rho_g} \quad ; \quad h=Y_g h_g+Y_l h_l \qquad (7)$$

The mixture thermodynamic properties and thermo - dynamic derivatives can be obtained by differentiating Equations (6) and (7) with respect to p and T such as Also, J is the transformation matrix. U and V are the contravariant velocities; the mixture flow viscosity is represented as $\mu = (1-\alpha)(1+2.5\alpha)\mu_\ell + \alpha\mu_g$ and α_i stands for volume fraction of each material. As usual, $\alpha \in [0, 1]$ and α represents the volume fraction of gas phase and (1-α) denotes the volume fraction of liquid phase; respectively. The volume fractions are assumed as one when the mixture flow is pure gas. Regarding the models of the saturation process among the steam-water mixture flows, the EOS for states of water, vapor and saturation modified from [13, 18] are selected together to yield a smooth link at the so-called spinodal points or the extreme points on the both sides of the saturation zone in the temperature-pressure diagram. They are

Liquid Phase EOS

A widely used EOS for water flow is the so–called Tait equation. This EOS was considered the water as a compressible fluid. The relation between the pressure and density is given as

$$P = B\left\{\left[\frac{\rho}{\rho_{tsat}}\right]^n - 1\right\} + P_{sat} \qquad (9)$$

Where P_{sat} is the temperature-dependent saturation pressure and the $\rho_{sat}(T)$ is the corresponding saturation density respectively. Also, $n = 7$ and $B = 3.3\times10^8$ Pa are chosen for water. Eq. (4) can be regarded as a family of self-similar curves in the (P, ρ) plane for pure liquid water phase. The speed of sound of water described in this EOS can be derived as

$$a = \sqrt{\frac{n}{\rho_{tsat}}(P+B)} \qquad (10)$$

Gas-Phase EOS

For water in its vapor phase, the ideal gas EOS is used like

$$P = \rho RT \qquad (11)$$

where $R = \hat{R}/\hat{M}$ represents the gas constant ($\hat{R}$ is the universal constant and $\hat{M}$ the molar mass). The speed of sound of the vapor can be derived as

$$a = \sqrt{\frac{\gamma P}{\rho}} \qquad (12)$$

with γ=1.4.

Saturation EOS

The saturation region is assumed to be in equilibrium: $P_l = P_g = P$ and $T_l = T_g = T$, where the pressure equals the saturated pressure $P = P_{sat}(T)$, and the temperature is equal to the saturation temperature $T = T_{sat}$. The saturation pressure and density can be obtained respectively as

$$\frac{P_{sat}(T)}{1MPa} = \left[\frac{2C}{-B+(B^2-4AC)^{0.5}}\right]^4 \qquad (13)$$

where

$$A = \vartheta^2 + n_1\vartheta + n_2\,,\ B = n_3\vartheta^2 + n_4\vartheta + n_5$$
$$C = n_6\vartheta^2 + n_7\vartheta + n_8 \qquad (14)$$

and the liquid and gas densities along the saturation curve are also chosen from [18] like

$$\frac{\rho_{tsat}(T)}{\rho_c} = 1 + b_1\theta^{\frac{1}{3}} + b_2\theta^{\frac{16}{3}} + b_5\theta^{\frac{43}{3}} + b_6\theta^{\frac{110}{3}} \qquad (15)$$

$$\ell n\left[\frac{\rho_{gsat}(T)}{\rho_c}\right] = c_1\theta^{\frac{2}{6}} + c_2\theta^{\frac{4}{6}} + c_3\theta^{\frac{8}{6}} + c_4\theta^{\frac{18}{6}} + c_5\theta^{\frac{37}{6}} + c_6\theta^{\frac{71}{6}} \qquad (16)$$

Where $\vartheta = \frac{T}{1K} + \frac{n_9}{\frac{T}{1K} - n_{10}}$ and the remained coefficients are seen in [18].

The corresponding enthalpy for the vapor phase and liquid phase for water become

$$h = C_p(T) + \frac{p}{\rho} \qquad (17)$$

where C_p is the specific heat coefficients at constant pressure can be found in [26]. Based on the above formulation (9-18), the diagrams of speed of sound to the gas volume fraction and the pressure to density for temperature=300k are depicted in Figure 1 and Figure 2, respectively. It is shown that the speed of sound is near 1500 m/s for a pure liquid, the speed of sound for a pure vapor is over 400 m/s and the minimum effective speed of sound of the saturated flow is below 5 m/s. Also from Figure 2, we can see the curve of pressure to density on the diagram is convex and connected smoothly.

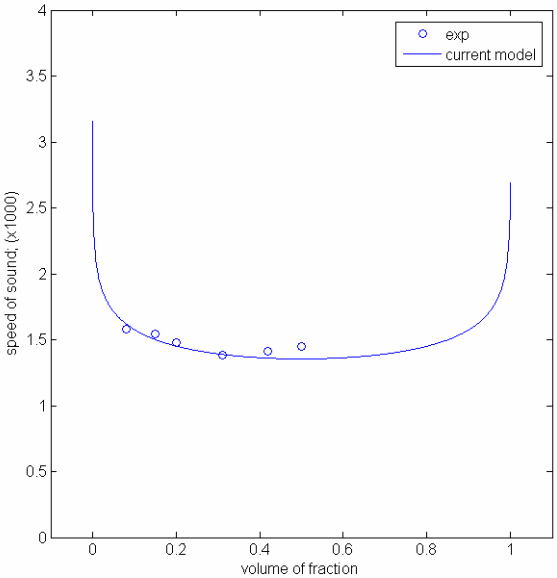

Figure 1 sound speed vs. gas volume fraction diagram at T=300K

Eigensystem of inviscid flux

In the work，the convective flux of the preconditioned governing equation can be linearized based on on the preconditioning matrix as

$$\Gamma=\begin{pmatrix} \theta & 0 & 0 & 0 & \rho_T & \rho_Y \\ u\theta & \rho & 0 & 0 & u\rho_T & u\rho_Y \\ v\theta & 0 & \rho & 0 & v\rho_T & v\rho_Y \\ w\theta & 0 & 0 & \rho & w\rho_T & w\rho_Y \\ H\theta-1 & u\rho & v\rho & w\rho & \rho_T H+\rho h_T & H\rho_Y+\rho h_Y \\ Y\theta & 0 & 0 & 0 & \rho_T Y & \rho+Y\rho_Y \end{pmatrix} \quad (18)$$

Here, we choose

$$\theta=\left(\frac{1}{U_r^2}-\frac{\rho_T}{\rho h_T}\right)\ ;\ U_r=\begin{cases} \varepsilon c, & \text{if } |U|<\varepsilon c \\ |U|, & \text{if } \varepsilon c<|U|<c \\ c, & \text{if } |U|>c \end{cases};\ i=1,2,3 \quad (19)$$

The inviscid flux Jabcobian $A=\Gamma^{-1}\dfrac{\partial F}{\partial W}$ and it's four distinct eigenvalues；The preconditioned Jacobian system $\tilde{A}_\Gamma$ has 6 eigenvalues as

$$\Lambda_\Gamma=\begin{pmatrix} \lambda_1 & 0 & 0 & 0 & 0 & 0 \\ 0 & \lambda_2 & 0 & 0 & 0 & 0 \\ 0 & 0 & \lambda_3 & 0 & 0 & 0 \\ 0 & 0 & 0 & \lambda_4 & 0 & 0 \\ 0 & 0 & 0 & 0 & \lambda_5 & 0 \\ 0 & 0 & 0 & 0 & 0 & \lambda_6 \end{pmatrix} \quad (20)$$

with

$$\lambda_1,\lambda_2,\lambda_3,\lambda_6=U,\qquad \lambda_4=U'+c',\qquad \lambda_5=U'-c'$$

here

$$U'=U(1-\alpha)\ ;\ c'=\sqrt{\alpha^2U^2+U_r^2} \quad (21)$$

α is defined as

$$\alpha=\left(1-\beta U_r^2\right)/2\ ;\ \beta=\rho_p+\frac{\rho_T}{\rho h_t}$$

Spatial Difference：

Considering the derivative of the convective flux in the ξ -direction, we use the following difference formula for the flux derivatives:

The convective flux at the cell interfaces is computed by the Roe type flux-difference splitting. The flux difference splitting scheme is constructed based on the eigenvalues and eigenvectors of the Jacobian matrix $\tilde{A}$. This approach admits that numerical flux F contains the characteristic information propagating through the domain, with speed and direction according to the eigenvalues of the system. By splitting F into parts, where each part contains the information traveling in a particular direction, i.e., characteristic information, and the split fluxes are differenced according to the directions of the corresponding wave propagation, the interface numerical flux of each cell is then expressed as

The evolution of the residual of the primitive variable W at each grid cell (i , j) is approximated by a third-order TVD Runge Kutta explicit time-marching scheme performed as

$$W^{(1)}=W^n-\Delta t\Gamma L(Q^n)$$

$$W^{(2)} = \frac{3}{4}W^n - \frac{1}{4}\{W^{(1)} - \Delta t\Gamma L(Q^{(1)})\} \quad (22)$$
$$W^{n+1} = \frac{1}{3}W^n + \frac{2}{3}\{W^{(2)} - \Delta t\Gamma L(Q^{(2)})\}$$

Where

$$L(W) = ((E^n_{i+1/2}(W^L_{i+1/2}, W^R_{i+1/2}) - E^n_{i-1/2}(W^L_{i-1/2}, W^R_{i-1/2})) - S(W^n_i)) \quad (23)$$

here：he interface conservative variables $W^L_{1+1/2}, W^R_{i+1/2}$ can be determined through the MUSCL approach [27] with the minmod limiter to achieve second-order or third-order spatial accuracy. Subsequently, the flux extrapolation of $F^n_{i+1/2}$ based on AUSMD type scheme is utilized to discretize the convective fluxes of mass, momentum, energy. The discretization of numerical flux is described in the following section, namely;

Results and Discussions

Quasi-One-Dimensional Nozzle

In the second case, a quasi-one-dimensional compressible liquid water nozzle is considered as shown in [20]. The inlet pressure condition is chosen as p =40 millions Pa, T =300 K, and u = 10 m/s, also the nozzle exit pressure is chosen set to 0.7 times the inlet pressure. This problem describes the phase transition process of a compressible water nozzle flow due to the rapid pressure drop to the saturated vapor after passing steep contraction in the nozzle throat. Numerical validation is performed on the mesh with 201 grid points. Also CFL number of 0.5 is chosen to keep the stability of the computations. Figure 4 (A) presents a simulated cavitation zone at the throat area with a very low pressure under the vapor pressure 3267 pa. Also a shock-like interface between the cavitation zone and condensation zone is captured without unwanted numerical spike errors after the flow passing through the throat area In Figure 4 (B), it is seen that the liquid water density in the throat area is monotonically decreased and coming with a sharp condensed shock wave in the recompression of the high pressure liquid state near the exit. A consistency is seen in the grid independence study on 401 and 801 grid points.

2-D injection nozzle

In the third test case, the following parameters are treated as variables in the simulations: the needle lift (H/D), and nozzle aspect ratio (L/D) as shown in Figure. 5 where $P_{0,}$ $P_{v,}$ P_∞ are injection pressure, vapor pressure, and back pressure respectively. Since the injection pressure is high (150 bar) in our simulations, the cavitation number for all cases is around unity. Numerical results shows that the cavitated nozzle flows are simulated under the vapor-water density ratio is up to 1:1000 and vapor density 0.86 (kg/m^3), Kinematics viscosity 9.18e-6 (kg/ms), injection pressure (150 bar) and the ratio L/D of 10. It is clearly simulated that at early injection stage, cavitation incepts at the inlet corner of nozzle orifice, extends downstream to the nozzle exit, and then shrinks back and collapses when the high pressure drop. An evolution of volume fraction for the vapor phase in a nozzle is captured around the turning corner in Figure 6 under the T=300k and U=10 m/s pressure drops of 1 Mpa with 1×10^5 Reynolds number. The occurrence of the cavitation is shown to begin with the cavitation number 1.252. It is seen that the cavitated area is getting larger as the pressure drop increases at the initial stage. The current cavitation model employed in the present study gives encouraging results for cavitating flows through nozzle for high pressure drop.

2-D Blunt Body Flow

Before performing the last case, we define the cavitation number by

$$\mathrm{K} = \frac{P_0 - P_v}{1/2(\rho U_0^2)} = \frac{P_0 - P_v}{P_0 - P_\infty} \quad (24)$$

Where P_0 , P_V , P_∞ are total pressure, saturated-vapor pressure, and free-stream pressure respectively. The last case corresponds to an experiment conducted by Rouse and McNown [28], involving liquid water flows over a hemisphere is performed. Initial conditions are assumed for each case with the same Reynolds number of 1.36×10^5 , temperature of 300 K, incoming uniform velocity of 4.317 m/s, but different cavitation numbers (K). The grid contains 300 x 85 nodes used in works of Edwards' works [20] , more details of flow conditions can be found in [20]. The influence the cavitation number on occurrence of cavitation is simulated. As the experimental data , the pressure in the expansion region drops to the vapor pressure in the cases of the cavitation number less than 0.8, resulting in the generation of a vapor phase and the growth of a cavitation bubble. As shown in Figures 7 (A), the evolutions of the cavitation zone in the density contour plots captured for the cases with K=0.2 to 0.4 and demonstrated by the computed density fields. Figures 7 (B) & (C) demonstrated that the data of surface pressure distributions which are compared with experimental data, also parameterized as functions of a cavitation number. As K decreases from 0.8, the pressure in the expansion region drops to the vapor pressure, resulting in the generation of a vapor phase and the growth of a cavitation bubble. Numerical validation with experimental data also shows that numerical accuracy decreases with the cavitation number increases. The current test results performed by the modified AUSMDV (new version) is shown to be consistent with the validated data when the K=0.4 and K=0.8 However, predicted surface pressure coefficients in the larger occurrence of bubble regions at the cases of

K=0.2 & K=0.3 do not completely agree with the experimental data, but demonstrate in a satisfactory tendency.

Concluded Remarks

In this work, a modification of the AUSMDV scheme based on the preconditioning scaled techniques is shown to be robust and accurate in the solving an all-speed type compressible cavitated water-vapor flow model with VOF type phase transition effects. Numerical validations are performed on the cases of an unsteady 1D shock-condensation tube and a quasi-1D nozzle flow. Also, the modified AUSMDV achieves robust and stable calculations of the cavitation phenomena in the 2D injector nozzle and blunt body flows. Though the turbulence effects are not considered in our computations, numerical validation against experimental data in the simulation of blunt body flows is satisfactory and demonstrates a very similar surface pressure coefficient prediction as the data of Rouse and McNown [28]. A further work is required to study physical phenomena contain many sizes of length and time scales such as the turbulence effects and surface tension effects of bubbles.

Acknowledgments

We acknowledge financial support from the National Science Council under the project NSC 96-2623-7-216-001-D. We thanks the discussions about AUSM scheme with Dr. Meng S. Liou and the cavitations models with Prof. Jack Edwards, also the computer facility supported by the National Center for High-Performance Computing, Hsin-Chu, Taiwan, ROC

References

[1] Wang, G., Senocak, I., Shyy, W., Ikohagi, T., Cao, S., *Progress in Aerospace Sciences*, Vol.37(2001), pp.551-58.

[2] Chen, Y., and Heister, S.D., "Two-Phase Modeling of Cavitated Flows," *Computers & Fluids*, Vol.24, (1995), pp.799-809

[3] L. Van Wijngaarden, One-dimensional flow of liquids containing small gas bubbles, *Annu. Rev. Fluid Mech.***4**, 369 (1972)

[4] H. B. Stewart, B. Wendroff, Two-phase flow: models and methods, Journal of Computational Physics 56 (1984) 363–409.

[5] W. Hirt, B. D. Nichols, "Volume of fluid method for the dynamics of free boundaries", Journal of Computational Physics 39 (1981) 201–225.

[6] Son., G., "Efficient implementation of a coupled level-set and volume-of-fluid method for three-dimensional incompressible two-phase flows", Numerical Heat Transfer, Part B; Fundamentals 43 (6), pp. 549-565, 2003

[7] M. Sussman, P. Smereka, S. Osher, "A level set approach for computing solutions of incompressible two-phase flows" , Journal of Computational Physics 114 (1994) 146–159

[8] Zheng, L.-L., Zhang, H., An adaptive level set method for moving-boundary problems： Application to droplet spreading and solidification, Numerical Heat Transfer, Part B; Fundamentals 37 (1-4), pp. 437-454, 2000

[9] Son., G., Hur, N., "A coupled level set and volume-of-fluid method for the buoyancy-driven motion of fluid particles", Numerical Heat Transfer, Part B; Fundamentals 42 (6), pp. 523-542, 2002

[10]Son., G., "A level set method for incompressible two-fluid flows with immersed solid boundaries", Numerical Heat Transfer, Part B; Fundamentals 47 (5), pp. 473-489, 2005

[11]R. J. Leveque, K. M. Shyue, "Two-dimensional front tracking based on high resolution wave propagation methods ", Journal of Computational Physics 123 (1996) 354–368.

[12]R. Saurel, and R. Abgrall, A simple method for compressible multifluid flows, SIAM J. Sci. Comput. 21 (3) (1999) 1115–1145.

[13]Saurel, R., and Cocchi, J.P., "Numerical Study of Cavitation in the Wake of a Hypervelocity Underwater Projectile," *Journal of Propulsion and Power*, Vol. 15, No. 4, 1999, pp. 513-522

[14]D. Pan, C. H. Chang, "The capturing of free surfaces in incompressible multi-fluid flows", International Journal for Numerical Methods in Fluids 33 (2000) 203–222.

[15]Jack R. Edwards, Randall K Franklin and Meng-Sing Liou, "Low-Diffusion Flux-Splitting Methods for Real Fluid Flows with Phase Transitions", *AIAA Journal,* pp1624–1633, 38, 2000

[16]M. D. Neaves and Jack R. Edwareds, "Time-Accurate All-Speed Multiphase Calculations Using A Low-Diffusion Flux Splitting Scheme", AIAA paper 04-1282, 42nd AIAA Aerospace Meeting , Reno, USA (2004)

[17]Yang-Yao Niu, "Simple Conservative Flux Splitting for Multi-component Flow Calculations", *Numerical Heat Transfer*, Part B, Vol.38 No. 2, pp.203-222, September, 2000

[18]Yang-Yao Niu, "A Simple and Robust Advection Upwind Flux Splitting to Simulate Transient Cavitated Water-Vapor Flows", *Numerical Heat Transfer*, Part B, Volume 51, Issue 7, January 2007 , pages 679 – 696

[19]Meng Sing Liou and Y. Wada, A Quest Towards Ultimate Numerical Flux Schemes, in M. Hafez and K. Oshima (eds.), Computational Fluid Dynamics Review 1995, pp. 251-278, Wiley, New York,1995

[20]Jack R. Edwards and Meng-Sing Liou, "Low-Diffusion Flux Splitting Methods for Flows at All Speeds, *AIAA Journal,* pp1610–1617, 38, 1998.

[21]C.-H. Chang and M.-S. Liou, A New Approach to the Simulation of Compressible Multifluid Flows with AUSM+ Scheme, AIAA 2003-4107.

[22]Handbook of 'IAPWS-IF97, Bernhard Spang, Hamburg, Germany,1997

[23]C. L. Merkle, J. Z. Feng, and P. E. O. Buelow, Computational modeling of the dynamics of sheet cavitation,in Proceedings of the 3rd International Symposium on Cavitation, Grenoble, France (J. M. Michel and H. Kato, Eds., 1998).
[24]I. Senocak and W. Shyy, A Pressure-Based Method for Turbulent Cavitating Flow Computations, AIAA Paper 2001-2907 (2001)
[25]J.W. Lindau, R. F. Kunz, D. A. Boger, D. R. Stinebring, and H. J. Gibeling, High Reynolds Number, unsteady multi-phase CFD modeling of sheet cavitation, J. Fluid Eng.-T ASME, **124**(3), (2002)
[26]V. Ahuja, A. Hosangadi and S. Arunajatesan, "Numerical Study of Cavitation in Cryogenic Fluids," Journal of Fluids Engineering, June 2001, Vol. 123, pp. 331-340
[27]A. Hosangadi and V. Ahuja, "Numerical Study of Cavitation in Cryogenic Fluids," Journal of Fluids Engineering, March 2005, Vol. 127, pp. 267-281
[28]Van Leer, B. "Towards the ultimate conservative difference, V: A second order sequel to Godunov's method", Journal of Computational Physics, Vol 32, pp.179-186, 1979
[29]Rouse, H., and McNown, J. S., "Cavitation and Pressure Distribution: Head Forms at Zero Angle of Yaw," State Univ. of Iowa Engineering Bulletin 32, Ames, IA, 1948.

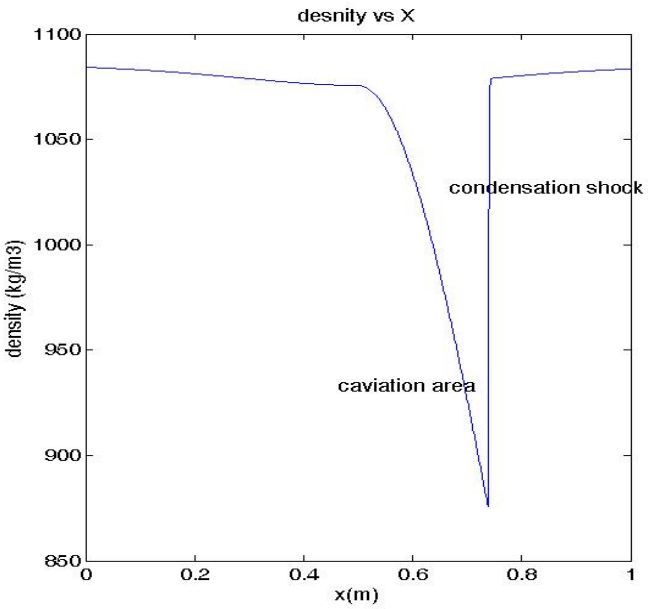

(B) the density distributions vs x

Figure 2 The diagram of a quasi-1D cavitated nozzle.

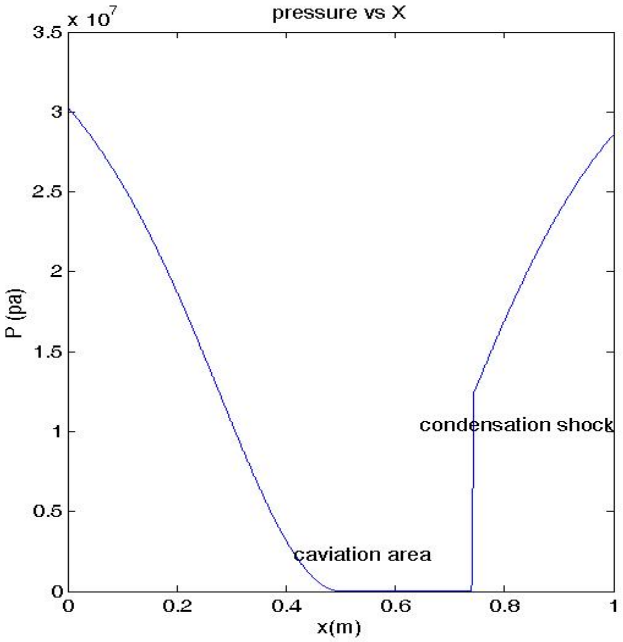

(A) the pressure distribution vs. x

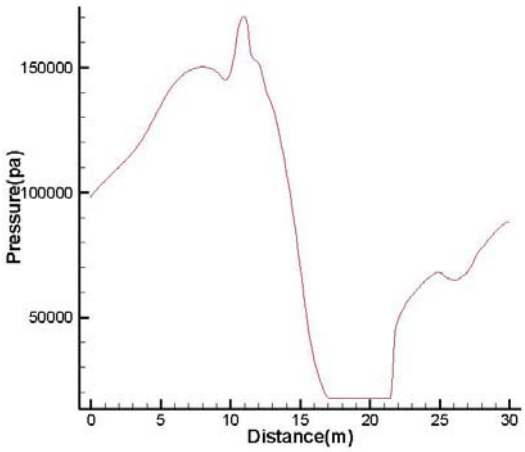

(A) the pressure distribution vs. distance

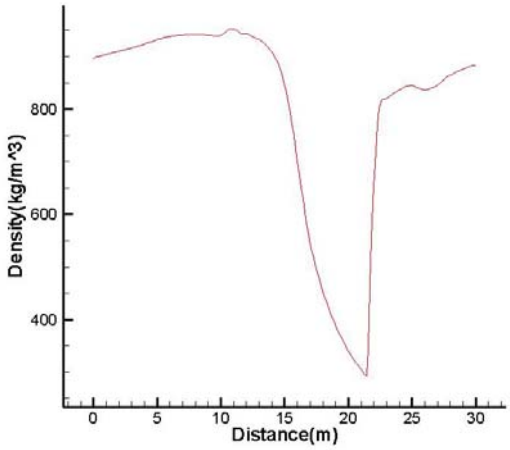

(B) the density distribution vs. distance

Figure 3 The diagram of a quasi-2D cavitated nozzle.

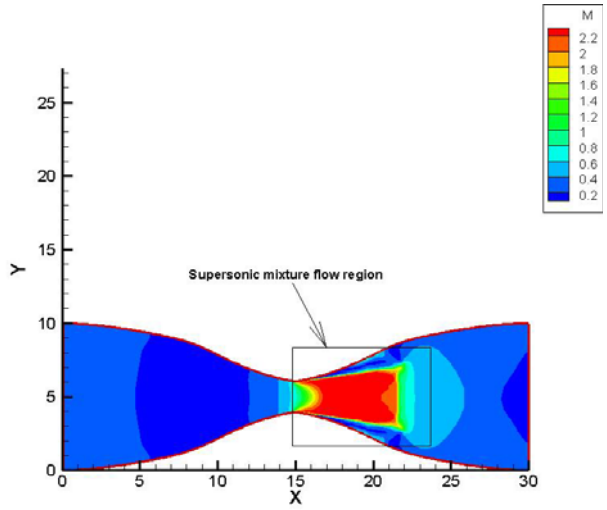

(A)

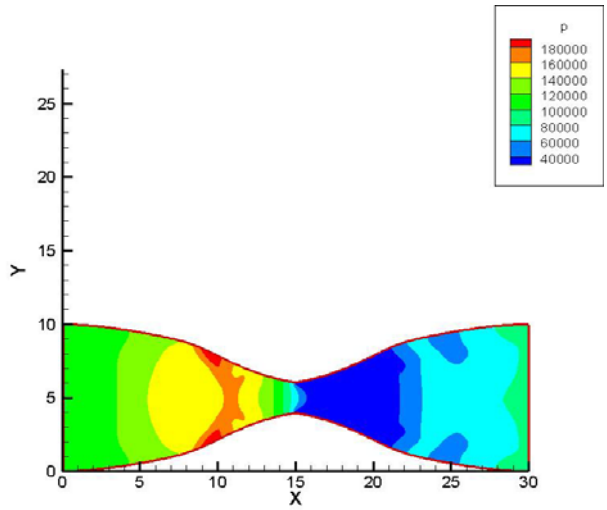

(B)

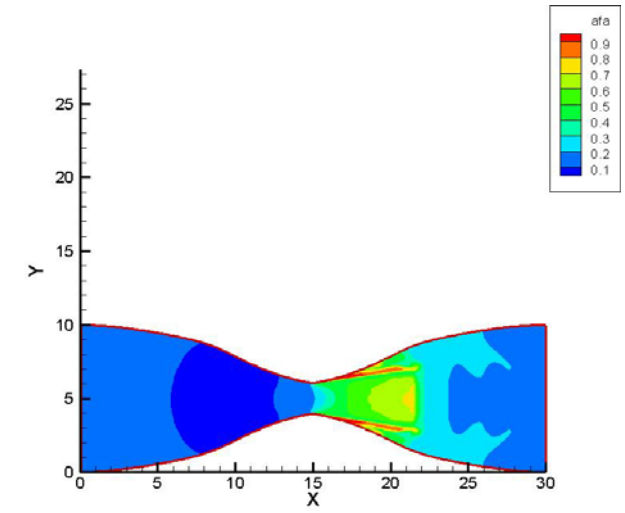

(C)

Figure 4 The diagram of a quasi-2D cavitated nozzle.

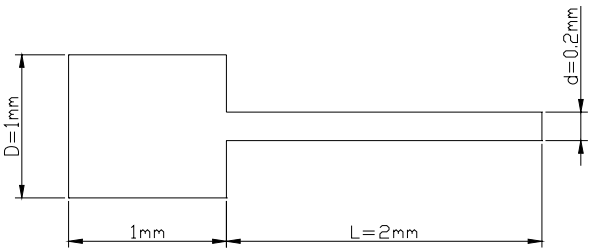

Figure 5 The diagram for a nozzle injector.

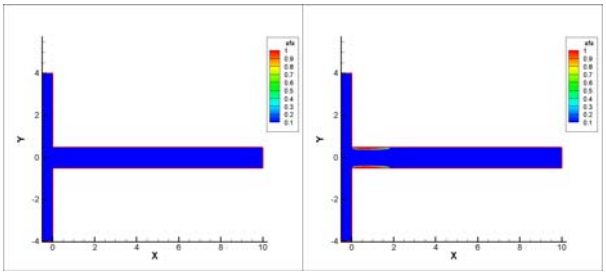

(1) (2)

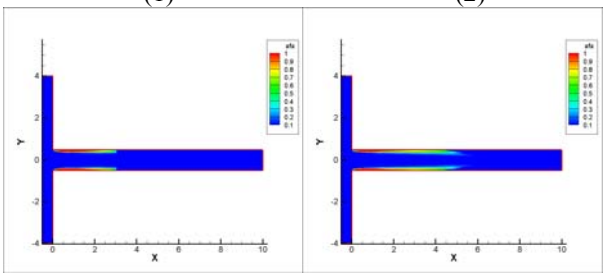

(3) (4)

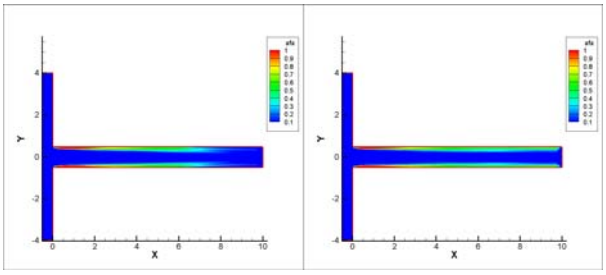

(5) (6)

Figure 6 an evolution of cavitated vapor-water in a nozzle under T=300K, U=10 m

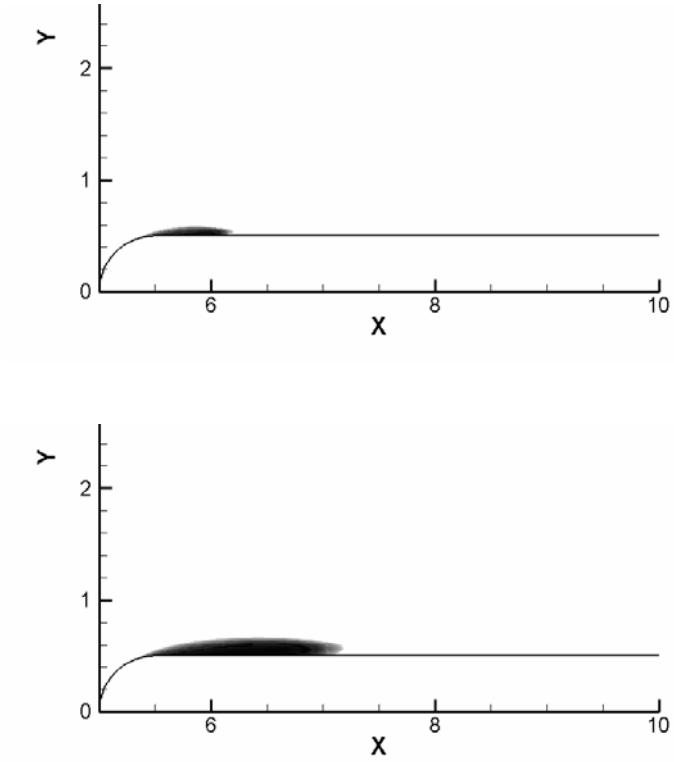

(A) the volume of fraction of gas phase contour plot

Figure 7 a cavitated vapor-water flow over an 2D blunt body under T=300K, U=4.317 m/s

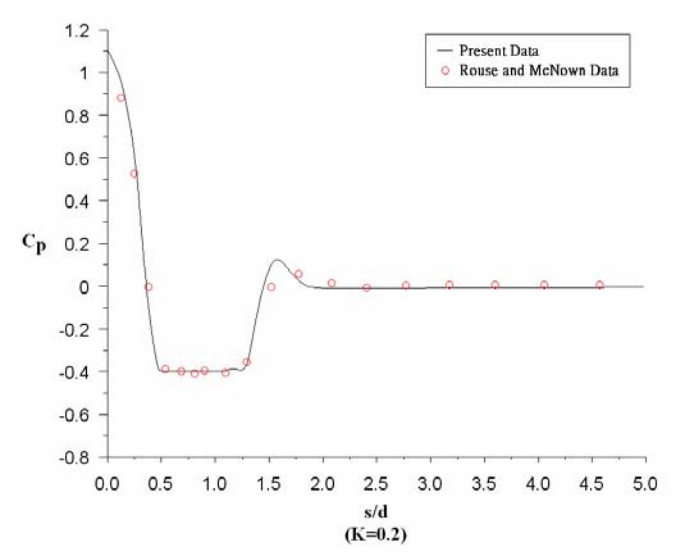

T=0.5 s

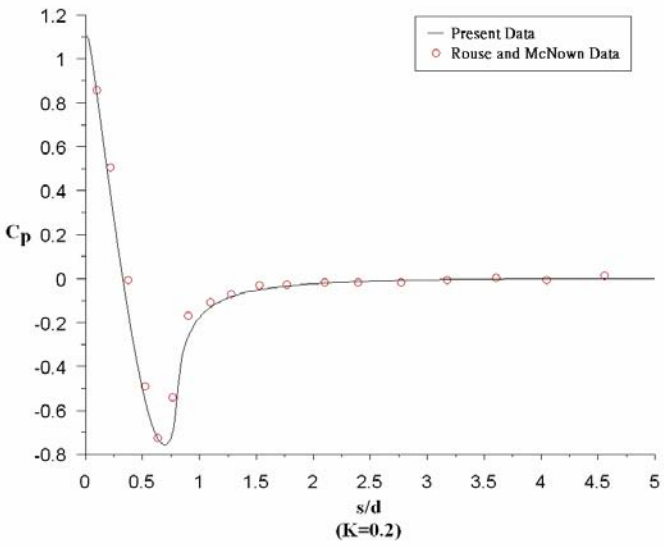

T=1.0 s